Estimation of the paramaters of a LVAC cable for a LVDC grid application

Ferréol Binot, Frédéric Reymond-Laruina, Loïc Queval, Marc Petit

ESTIMATION OF THE PARAMETERS OF A LVAC CABLE FOR A LVDC GRID APPLICATION

Ferréol BINOT
Centrale Lille – L2EP – France
ferreol.binot@centralelille.fr

Frédéric REYMOND-LARUINA
EDF R&D – France
frederic.reymond-laruina@edf.fr

Loïc QUEVAL and Marc PETIT
CentraleSupélec – GeePs – France
{loic.queval, marc.petit}@centralesupelec.fr

ABSTRACT

Despite the rise of LVDC grids, the type of cable to use is still debated. An interesting solution would be the reused AC cables. Through experimental measurements and comparison with an analytical model, this works provides values for steady state and transient analysis of a French distribution cable in DC grids.

INTRODUCTION

In response to the climate emergency [1], new applications, including photovoltaic panels (PV), electrical mobility, and heat pumps, have been introduced on the distribution grid [2], [3]. Most of these new uses are powered in DC or via converters that go through a DC level. To reduce grid losses and the number of converters, the question arises of developing Low Voltage Direct Current (LVDC) grids. For economic reasons, using existing cables in DC seems preferred. Indeed, existing Low Voltage Alternative Current (LVAC) cable are already characterized for voltage operation up to 1500 V RMS, according to IEC 60050. Therefore, the highest possible voltage is 1800 V [4]. The absence of reactive power, as well as the lower DC resistance, allows DC cable to transmit more power. The actual limit being the cable core temperature which shouldn't exceed 90°C [5], [6].

In the literature, several authors propose to convert AC cables to DC cables. The AC2DC project aims to develop DC links for the German distribution grid [7]. German distribution system operators are surveyed to find out currently used cable technologies and their potential of conversion to DC. For example, a 0.6/1 kV LVAC cable can transfer at least double power in DC. To test the cable performance, FEM modelling and experiments were performed to determine the temperature of the cable in service, showing the importance of knowing the values of the parameters of these cables. Similarly the ANGLE DC project aims to develop a MV DC link between the island of Anglesey and the Welsh mainland [8]. Three phases are connected in parallel to provide one pole. This project wanted to demonstrate the feasibility of a DC link using existing AC cable. In [9], the authors analyses several methods of converting AC MV lines to DC lines, as well as their control methods, in order to increase the transfer capacities. Relations are given to estimate parameters and losses in steady state operation. In a similar way, [10] performed a techno-economic analysis of a LVAC grid compared to the same grid in DC. Assuming the 400 V AC cable can be operated at a higher voltage, the maximum transmitted power is multiplied by about 4 between AC and DC solutions. Both studies underline the advantage of using the current AC cables in DC. Nevertheless, the authors scarcely determine impedance of the cables and focus mainly on steady state analysis. [11], [12] propose more complete models, but are limited to HVDC cables configuration.

Analysis of the above literature draws attention to several aspects that are insufficiently addressed. French cable, whose geometry is different from other countries, is never studied. Cable parameters are generally limited to the DC resistance and no value is provided for transient analysis. Our article offers to complete these gaps. In Section 2, the methodology to determine the LVAC cable parameters analytically and experimentally is described. Section 3 presents the characterization results on the French cable based on the proposed methodology and gives parameters to be exploited in later studies.

METHODOLOGY

Type of cable studied

In this article, we considered a typical 150/95 mm² French LV cable used in the distribution grid. This cable is composed of 3 sector conductors for phases a, b, and c and one circular conductor for the neutral completed by a crown that surrounds all the conductors. Depending on the grounding system of the DC grids, four conductors could be needed, as well as three.

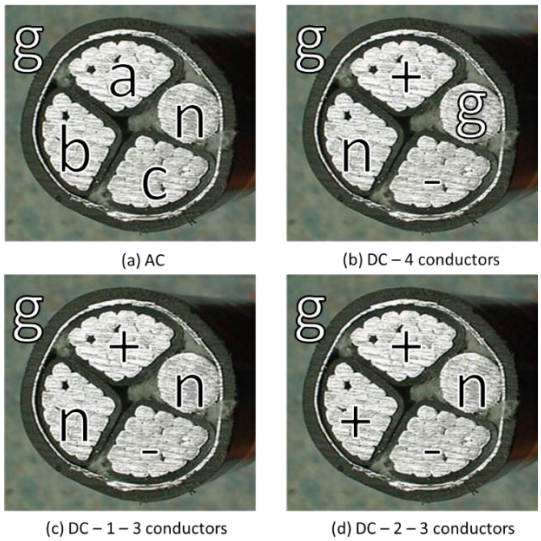

Figure 1. Pictures of the French LV cable for four configurations: (a) usual AC, (b) 4 conductors DC (b), (c) 3 conductors - option 1 and (d) 3 conductors - option 2

The different possibilities are represented in Figure 1. In this study, only configuration (b) and (c) are considered. They correspond respectively to a TN-S and TN-C-S grounding. Because we are interested in having symmetric poles, configuration (d) is not studied.

Analytical model

In [13], an analytical model of a four conductors LV cable has been developed. This model represents the configuration (a) of Figure 1 and allows to determine the impedance matrices at 50 Hz, as described on Figure 2.

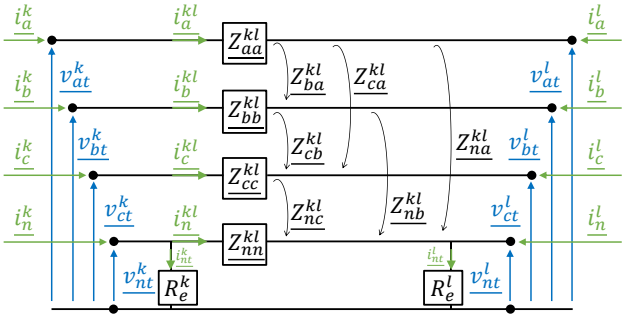

Figure 2. Analytical model of LV cable.

Based on this work, we extended the method for a variable frequency while maintaining the same relation (1).

$$\begin{bmatrix} \underline{v_{at}^{kl}} \\ \underline{v_{bt}^{kl}} \\ \underline{v_{ct}^{kl}} \\ \underline{v_{nt}^{kl}} \end{bmatrix} = \begin{bmatrix} \underline{v_{at}^{k}} \\ \underline{v_{bt}^{k}} \\ \underline{v_{ct}^{k}} \\ \underline{v_{nt}^{k}} \end{bmatrix} - \begin{bmatrix} \underline{v_{at}^{l}} \\ \underline{v_{bt}^{l}} \\ \underline{v_{ct}^{l}} \\ \underline{v_{nt}^{l}} \end{bmatrix} = \underbrace{\begin{bmatrix} \underline{Z_{aa}^{kl}} & \underline{Z_{ab}^{kl}} & \underline{Z_{ac}^{kl}} & \underline{Z_{an}^{kl}} \\ \underline{Z_{ba}^{kl}} & \underline{Z_{bb}^{kl}} & \underline{Z_{bc}^{kl}} & \underline{Z_{bn}^{kl}} \\ \underline{Z_{ca}^{kl}} & \underline{Z_{cb}^{kl}} & \underline{Z_{cc}^{kl}} & \underline{Z_{cn}^{kl}} \\ \underline{Z_{na}^{kl}} & \underline{Z_{nb}^{kl}} & \underline{Z_{nc}^{kl}} & \underline{Z_{nn}^{kl}} \end{bmatrix}}_{\underline{\boldsymbol{Z}}^{kl} = \underline{\boldsymbol{z}} \cdot l^{kl}} \begin{bmatrix} \underline{i_a^{kl}} \\ \underline{i_b^{kl}} \\ \underline{i_c^{kl}} \\ \underline{i_n^{kl}} \end{bmatrix} \quad (1)$$

To determine the DC parameters, we computed the matrix $\underline{\boldsymbol{z}}$ at 0.1 Hz in mΩ.km^{-1}. According to this result an estimation of the per-unit-length self-resistance would be 205 mΩ.km^{-1}, while the per-unit-length mutual and self-inductances would be of 2 mΩ.km^{-1}.

$$\underline{\boldsymbol{z}}_{0.1Hz}^{a} = \begin{bmatrix} 205+2j & 2j & 2j & 2j \\ 2j & 205+2j & 2j & 2j \\ 2j & 2j & 205+2j & 2j \\ 2j & 2j & 2j & 259+2j \end{bmatrix} \quad (2)$$

From the reference, the original matrix at 50 Hz is given below. A decrease in resistance and inductance can be noticed.

$$\underline{\boldsymbol{z}}_{50Hz}^{a} = \begin{bmatrix} 254+758j & 49+694j & 49+680j & 49+708j \\ 49+694j & 254+758j & 49+694j & 49+679j \\ 49+680j & 49+694j & 254+758j & 49+708j \\ 49+708j & 49+679j & 49+708j & 299+764j \end{bmatrix} \quad (3)$$

Because the analytical model cannot be used for a three conductors' configuration, like the configuration (c), it is proposed to approximate the impedance of the parallelized conductors as the two self-impedances in parallel.

Laboratory measurements

To validate the analytical model, the platform PHILibert is used to generate a power sinusoidal signal at different frequencies: 10 Hz, 30 Hz, 60 Hz, 120 Hz, 240 Hz and 480 Hz. 50 Hz is not considered to avoid the influence of the main grid noise. A step-down transformer is inserted in serial to increase the current and allow a voltage measurement. The 10 m cable was disposed in a perfect circle to minimize parasite inductance.

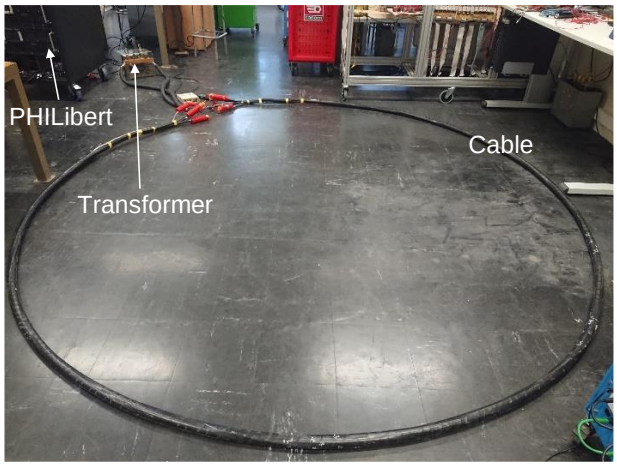

Figure 3. Experimental setup

When the phase a is supplied by the transformer, the parameters are determined using the following equations:

$$P_a = \frac{1}{T}\int_0^T i_a(t).v_a(t)dt \quad (4)$$

$$X_{aa} = \frac{\sqrt{(V_a.I_a)^2 - {P_a}^2}}{{I_a}^2} \quad (5)$$

$$L_{aa} = \frac{X_{aa}}{2\pi f} \quad (6)$$

$$R_{aa} = \frac{P}{{I_a}^2} \quad (7)$$

$$X_{ab} = \frac{V_b}{I_a} \quad (8)$$

Where P_a is the active power consumed in the phase a $[W]$, X_{aa} the self-reactance of phase a [Ω], L_{aa} the self-inductance of phase a [H], R_{aa} the resistance of phase a [Ω], X_{ab} the mutual reactance of phase a relatively to phase b [Ω], V_a the RMS voltage of phase a [V], V_b the RMS voltage of phase b [V], I_a the RMS current in phase a [A], f the frequency $[Hz]$, i_a the instantaneous current in phase a [A], v_a the instantaneous voltage of phase a [V].

The difference between the analytical and the measurements is quantified with the relative error given by:

$$\varepsilon = 100.\frac{V_{th} - V_{mes}}{|V_{mes}|} \quad (9)$$

Where V_{th} is the expected theoretical value of the studied parameter and V_{mes} the measured value of the studied parameter. With this formulation, having a positive error means that the theoretical value is higher than the measured value, while a negative error means the

theoretical value is lower than the measured value.

CABLE STUDY AND CHARACTERIZATION RESULTS

In this section, the impedances of configurations (b) and (c) are compared to the impedances obtained analytically.

Per-unit-length resistance

Each phase is characterized alone in a first time, to describe the configuration (b). The measurements of conductor resistance are given in Table 1.

Table 1 : Measured resistance in $m\Omega.km^{-1}$of each phase in configuration (b) and (c) according to the frequency. The superscript and the subscript of the resistance represent the configuration and the phase respectively.

	10	30	60	120	240	480
R_a^b	67.82	119.1	165.3	240.1	416.6	4066
R_b^b	74.79	118.8	151.9	246.7	531.3	3995
R_c^b	68.18	120.1	151.9	229.6	537.2	3876
R_n^b	123.6	198.9	234.8	247	716.6	4032
R_a^c	71.01	115.9	163.6	259.5	568	4054
R_{b+n}^c	23.54	54.45	88.91	180.2	431.3	3723
R_c^c	82.51	140.3	173.3	279.1	603.3	4144

Figure 4 depicted the relative error based on (9). Despite a high error at 480 Hz, the proposed method allows to get accurate results at all frequencies. At around 50 Hz, the results are more accurate than in [13]. The divergence of results for high frequencies can be due to the proximity or skin effects, which are not considered in (1). At 10 Hz, the transformer deforms the signals which leads to the sudden rise of error.

The measurements have been repeated for the configuration (c). The results are shown in Table 1. The resistance of conductors changes slightly for phase a and c, unlike phase b due to the connection in parallel of the neutral. This change cannot be predicted by the proposed model as illustrated by Err_{eq} of the Figure 5, which compares R_{b+n}^c with R_b^a and R_n^a in parallel.

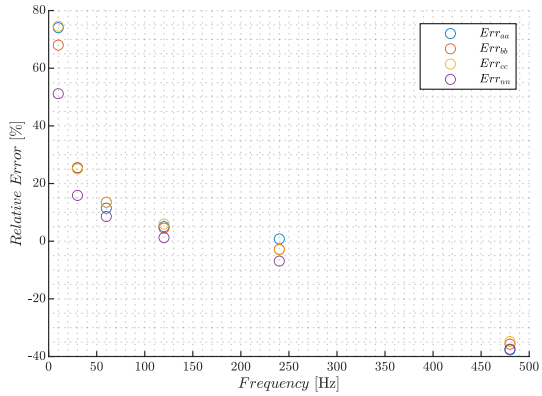

Figure 4 : Relative error for the characterization of phase resistance in configuration (b) compared to the analytical model

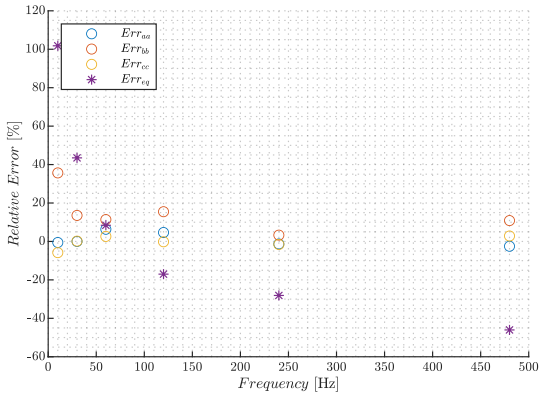

Figure 5 : Relative error for the characterization of phase resistance in configuration (c) compared to the measurement in configuration (b) for phase a, b, and c. Err_{eq} compares R_{b+n}^c with R_b^a and R_n^a in parallel.

To be able to give an estimation of the DC resistance from AC measurements, we propose to approximate the data by the following exponential function:

$$R(f) = R_{DC}.e^{\alpha.f} \quad (10)$$

Where R_{DC} is the DC resistance of the conductor $[\Omega.\mathrm{km}^{-1}]$, f is the frequency and α a coefficient depending on the conductor. The results are synthetized in Table 2.

Table 2 : Value of parameters of model proposed at (10) for configurations (b) and (c)

Phase	R_{DC} $[\mathrm{m\Omega.km^{-1}}]$	α $[s]$
Configuration (b)		
a	59	$8.8 \cdot 10^{-3}$
b	79	$8.2 \cdot 10^{-3}$
c	80	$8.0 \cdot 10^{-3}$
n	139	$7.0 \cdot 10^{-3}$
Configuration (c)		
a	86	$8.0 \cdot 10^{-3}$
b+n	51	$8.9 \cdot 10^{-3}$
c	96	$7.8 \cdot 10^{-3}$

Although values are close, the resistance is different for every phase. This phenomenon was already shown in Figure 5. In a first approximation, it can be considered that in configuration (b), average phase DC resistance is $73\ \mathrm{m\Omega.km^{-1}}$, while the neutral DC resistance is $139\ \mathrm{m\Omega.km^{-1}}$. In configuration (c), the average phase resistance is $91\ \mathrm{m\Omega.km^{-1}}$, while the equivalent resistance of parallel conductor is $51\ \mathrm{m\Omega.km^{-1}}$. These values are far from the analytical one. To validate these results a third measure, through a DC source has been performed. In summary, this measure confirms the analytical result with an average resistance of $196\ \mathrm{m\Omega.km^{-1}}$ for phases.

In case of a transient study, like a pole to pole short-circuit, it is more relevant to consider an average value of the

resistance measured between 30 Hz and 120 Hz: the oscillating phenomenon occurring around these frequencies. In configuration (b), average phase resistance is $148\ \mathrm{m\Omega.km^{-1}}$ and the neutral resistance values $226\ \mathrm{m\Omega.km^{-1}}$. In configuration (c), the average phase resistance is $152\ \mathrm{m\Omega.km^{-1}}$ and the equivalent resistance of parallel conductor values $87\ \mathrm{m\Omega.km^{-1}}$.

Per-unit-length inductance

Concerning the characterization of the cable self-inductance, the results are shown in Table 3 for configurations (b) and (c).

Table 3 : Measured self-inductance in $mH.km^{-1}$ of each phase in configuration (b) and (c) according to the frequency

	10	30	60	120	240	480
L_a^b	2.95	2.32	2.24	2.15	2.08	2.66
L_b^b	3.04	2.31	2.16	2.02	2.09	2.78
L_c^b	2.92	2.33	2.16	2.05	2.09	2.75
L_n^b	3.69	2.42	2.16	2.09	2.17	2.61
L_a^c	2.97	2.31	2.11	2.06	2.11	2.73
L_{b+n}^c	2.24	2.04	1.94	1.91	2.02	2.51
L_c^c	3.11	2.32	2.1	2.06	2.12	2.69

The relative errors are presented in Figure 6 and Figure 7.

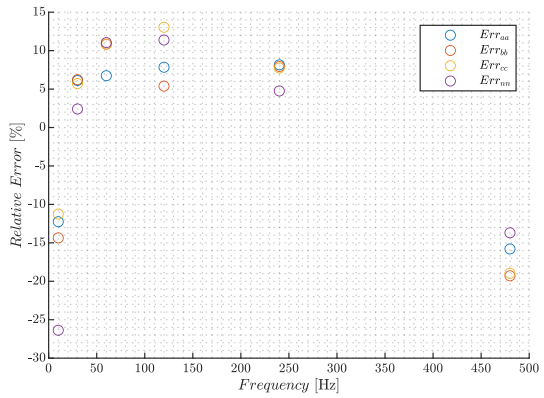

Figure 6 : Relative error for the conductor self-inductance in configuration (b) compared to analytical model

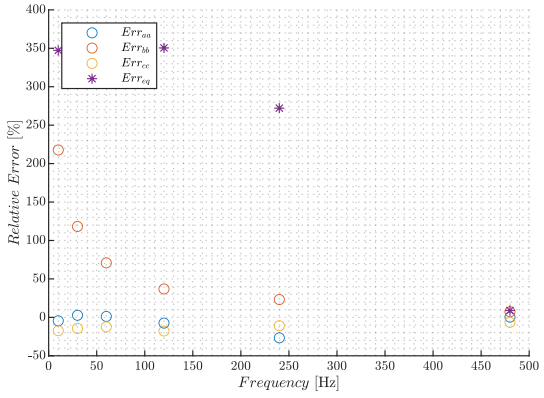

Figure 7 : Relative error for the characterization of phase self-inductance in configuration (c) compared to the measurement in configuration (b) for phase a, b, and c. Err_{eq} compares R_{b+n}^c with R_b^a and R_n^a in parallel.

As for the resistance estimation, it appears that the model has a good accuracy for frequency between 30 Hz and 240 Hz. However, whatever the frequency, the absolute relative error stays between 18 % and 3 % which is better than for the resistance estimation. Furthermore, changing the conductors' configuration changes the inductance value for the parallelised conductors, while it remains almost constant for the others. Figure 7 demonstrates that the value of the self-inductance these last conductors cannot be predicted with the hypothesis made.

As the self-inductance is a parameter mostly used for transient analysis [14], only the average value around 50 Hz is computed. Thus, in configuration (b), phases and neutral conductor inductances is around $2.4\ \mathrm{mH.km^{-1}}$. In configuration (c), the value of the parallelized conductors decreases to $2.1\ \mathrm{mH.km^{-1}}$.

Per-unit-length mutual inductance

Figure 8 shows relative error between the analytical model and the measurements in configuration (b) for mutual inductance value.

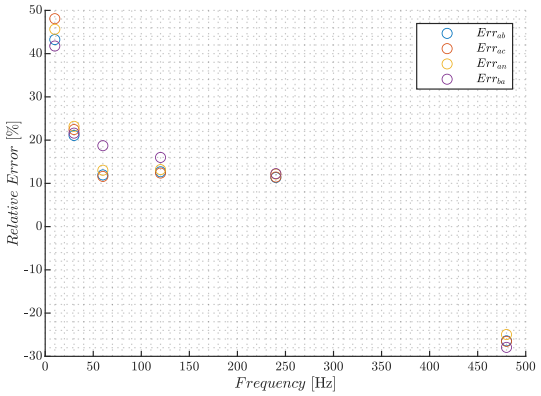

Figure 8 : Relative error of mutual inductance in configuration (b) compared to analytical model

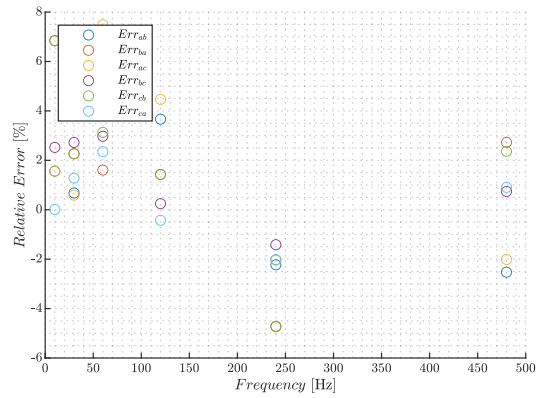

Figure 9 : Relative error of mutual inductance between configurations (c) and (b)

A small difference of mutual inductance can be note: $X_{ab}^{b} \neq X_{ba}^{b}$, unlike the analytical model. Apart from that and based on the same method as previously, an average value of the mutual inductance is $1.9\,\mathrm{mH.km^{-1}}$ for configuration (b). Based on Figure 9, where the error is on average 3%, it can be inferred that almost no divergence of results exists between configuration (b) and (c): the mutual inductance is similar whatever the configuration.

Proposed values

Table 4 and Table 5 summarize proposed values in this article for the studied distribution cable, depending on the analysis to perform.

Table 4 : Proposed values for steady state analysis

	Configuration (b)	Configuration (c)
Phase	$196\,\mathrm{m\Omega.km^{-1}}$	$196\,\mathrm{m\Omega.km^{-1}}$
Neutral	$139\,\mathrm{m\Omega.km^{-1}}$	$51\,\mathrm{m\Omega.km^{-1}}$

Table 5 : Proposed values transient analysis

		Configuration (b)	Configuration (c)
Phase	R	$148\,\mathrm{m\Omega.km^{-1}}$	$226\,\mathrm{m\Omega.km^{-1}}$
	L	$2.4\,\mathrm{mH.km^{-1}}$	$2.4\,\mathrm{mH.km^{-1}}$
	M	$1.9\,\mathrm{mH.km^{-1}}$	$1.9\,\mathrm{mH.km^{-1}}$
Neutral	R	$152\,\mathrm{m\Omega.km^{-1}}$	$87\,\mathrm{m\Omega.km^{-1}}$
	L	$2.4\,\mathrm{mH.km^{-1}}$	$2.1\,\mathrm{mH.km^{-1}}$
	M	$1.9\,\mathrm{mH.km^{-1}}$	$1.9\,\mathrm{mH.km^{-1}}$

CONCLUSION AND FUTURE WORKS

Parameters allowing to describe the behaviour of a French LV cable has been determined for steady state and transient analysis for two different configurations. The self and mutual inductance of each conductor is dedicated to transient analysis, while the resistance values concern steady state and transient analysis. An analytical model, validated by experimental measurements, allows to determine accurately all the parameters of the cable between 30 Hz and 120 Hz. At higher frequencies, only self and mutual inductance can be retrieved, because proximity and skin effect are not considered. As regards low frequencies, the DC resistance value offers a significant divergence between the analytical model and the measurements at 10 Hz. A test with a high DC current source allowed to validate the analytical value provided in this article. Further studies will be needed to understand the impact of parallelizing conductors.

REFERENCES

[1] V. Masson-Delmotte et al., Eds., Climate Change 2021: The Physical Science Basis. Contribution of Working Group I to the Sixth Assessment Report of the Intergovernmental Panel on Climate Change. Cambridge University Press, 2021.

[2] C. Protopapadaki and D. Saelens, “Heat pump and PV impact on residential low-voltage distribution grids as a function of building and district properties,” Applied Energy, vol. 192, pp. 268–281, Apr. 2017, doi: 10.1016/j.apenergy.2016.11.103.

[3] F. Gonzalez Venegas, M. Petit, and Y. Perez, “Active integration of electric vehicles into distribution grids: Barriers and frameworks for flexibility services,” Renewable and Sustainable Energy Reviews, vol. 145, p. 111060, Jul. 2021, doi: 10.1016/j.rser.2021.111060.

[4] S. Krahmer et al., “Conversion of Existing AC into DC Cable Links in Distribution Grids: Benefits and Challenges,” in ETG Congress 2021, Mar. 2021, pp. 1–6.

[5] ABB, “XLPE Submarine Cable Systems - Attachment to XLPE Land Cable Systems User’s Guide.” Accessed: Jan. 17, 2023. [Online]. Available: https://new.abb.com/docs/default-source/ewea-doc/xlpe-submarine-cable-systems-2gm5007.pdf

[6] NKT, “Câble de réseaux souterrain H1 XDV-AS.” Accessed: Oct. 20, 2020. [Online]. Available: https://www.smv-entreprise.fr/media/original/enedis-h1-xdv-as-33-s-210-221033.pdf

[7] Stephan Rupp, Sebastian Krahmer, Robert Adam, Karsten Backhaus, Christian Hildmann, and Matthias Nilges, “Conversion of Existing AC into DC Cable Links in Distribution Grids Benefits and Challenges,” 2021.

[8] J. Yu, K. Smith, M. Urizarbarrena, N. MacLeod, R. Bryans, and A. Moon, “Initial designs for the ANGLE DC project; converting existing AC cable and overhead line into DC operation,” in 13th IET International Conference on AC and DC Power Transmission (ACDC 2017), Manchester, UK, 2017, p. 2 (6 .)-2 (6 .). doi: 10.1049/cp.2017.0002.

[9] L. Zhang, J. Liang, W. Tang, G. Li, Y. Cai, and W. Sheng, “Converting AC Distribution Lines to DC to Increase Transfer Capacities and DG Penetration,” IEEE Trans. Smart Grid, vol. 10, no. 2, pp. 1477–1487, Mar. 2019, doi: 10.1109/TSG.2017.2768392.

[10] T. Kaipia, P. Salonen, J. Lassila, and J. Partanen, “Possibilities of the low voltage DC distribution systems,” Aug. 2006.

[11] W. Frelin and P. Egrot, “Key parameters for extruded DC cable qualification”.

[12] J. Yang, J. O’Reilly, and J. E. Fletcher, “An overview of DC cable modelling for fault analysis of VSC-HVDC transmission systems,” p. 5.

[13] Ferréol BINOT, “Modélisation et estimation de paramètres des réseaux de distribution basse tension,” Université Paris-Saclay, 2020.

[14] J. Yang, J. E. Fletcher, and J. O’Reilly, “Short-Circuit and Ground Fault Analyses and Location in VSC-Based DC Network Cables,” IEEE Trans. Ind. Electron., vol. 59, no. 10, pp. 3827–3837, Oct. 2012, doi: 10.1109/TIE.2011.2162712.